of the test set spike train under the predicted firing probability relative to a constant probability given by the mean firing rate on the training set. Computed to base 2, this ratio estimates the number of bits a communicator of the test set spike train can save by knowing the predictor variables (position and/or peer cell activity), as compared with knowing only mean rate. Spike rasters were re-ordered for display by stochastic search over all possible orderings, to maximize the fraction of spike pairs between neighbouring rasters that lay within 25 ms (Figs 1b and 4a).

See Supplementary Information for a full description of methods.

Received 14 April; accepted 9 June 2003; doi:10.1038/nature01834.

1. Mainen, Z. F. & Sejnowski, T. J. Reliability of spike timing in neocortical neurons. *Science* **268,** 1503–1506 (1995).
2. Hebb, D. O. *The Organization of Behavior* (Wiley, New York, 1949).
3. Freiwald, W. A., Kreiter, A. K. & Singer, W. Synchronization and assembly formation in the visual cortex. *Prog. Brain Res.* **130,** 111–140 (2001).
4. Engel, A. K., Fries, P. & Singer, W. Dynamic predictions: oscillations and synchrony in top-down processing. *Nature Rev. Neurosci.* **2,** 704–716 (2001).
5. O'Keefe, J. & Recce, M. L. Phase relationship between hippocampal place units and the EEG theta rhythm. *Hippocampus* **3,** 317–330 (1993).
6. Skaggs, W. E., McNaughton, B. L., Wilson, M. A. & Barnes, C. A. Theta phase precession in hippocampal neuronal populations and the compression of temporal sequences. *Hippocampus* **6,** 149–172 (1996).
7. Harris, K. D. *et al.* Spike train dynamics predicts theta-related phase precession in hippocampal pyramidal cells. *Nature* **417,** 738–741 (2002).
8. Mehta, M. R., Lee, A. K. & Wilson, M. A. Role of experience and oscillations in transforming a rate code into a temporal code. *Nature* **417,** 741–746 (2002).
9. Spruston, N. & Johnston, D. Perforated patch-clamp analysis of the passive membrane properties of three classes of hippocampal neurons. *J. Neurophysiol.* **67,** 508–529 (1992).
10. Csicsvari, J., Jamieson, B., Wise, K. D. & Buzsáki, G. Mechanisms of gamma oscillations in the hippocampus of the behaving rat. *Neuron* **37,** 311–322 (2003).
11. Magee, J. C. & Johnston, D. A synaptically controlled, associative signal for Hebbian plasticity in hippocampal neurons. *Science* **275,** 209–213 (1997).
12. Reinagel, P. & Reid, R. C. Precise firing events are conserved across neurons. *J. Neurosci.* **22,** 6837–6841 (2002).
13. Kara, P., Reinagel, P. & Reid, R. C. Low response variability in simultaneously recorded retinal, thalamic, and cortical neurons. *Neuron* **27,** 635–646 (2000).
14. Buracas, G. T., Zador, A. M., DeWeese, M. R. & Albright, T. D. Efficient discrimination of temporal patterns by motion-sensitive neurons in primate visual cortex. *Neuron* **20,** 959–969 (1998).
15. Fenton, A. A. & Muller, R. U. Place cell discharge is extremely variable during individual passes of the rat through the firing field. *Proc. Natl Acad. Sci. USA* **95,** 3182–3187 (1998).
16. Shadlen, M. N. & Newsome, W. T. Noise, neural codes and cortical organization. *Curr. Opin. Neurobiol.* **4,** 569–579 (1994).
17. Lisman, J. E. & Idiart, M. A. Storage of 7 ± 2 short-term memories in oscillatory subcycles. *Science* **267,** 1512–1515 (1995).
18. Redish, A. D. *et al.* Independence of firing correlates of anatomically proximate hippocampal pyramidal cells. *J. Neurosci.* **21,** RC134 [online] ⟨http://www.jneurosci.org/cgi/content/full/21/10/RC134⟩ (2001).
19. Hirase, H., Leinekugel, X., Csicsvari, J., Czurko, A. & Buzsáki, G. Behavior-dependent states of the hippocampal network affect functional clustering of neurons. *J. Neurosci.* **21,** RC145 [online] ⟨http://www.jneurosci.org/cgi/content/full/21/10/RC145⟩ (2001).
20. O'Keefe, J. & Nadel, L. *The Hippocampus as a Cognitive Map* (Clarendon, Oxford, 1978).
21. Wilson, M. A. & McNaughton, B. L. Dynamics of the hippocampal ensemble code for space. *Science* **261,** 1055–1058 (1993).
22. Brown, E. N., Frank, L. M., Tang, D., Quirk, M. C. & Wilson, M. A. A statistical paradigm for neural spike train decoding applied to position prediction from ensemble firing patterns of rat hippocampal place cells. *J. Neurosci.* **18,** 7411–7425 (1998).
23. Cox, D. R. & Isham, V. *Point Processes* (Chapman and Hall, London, 1980).
24. Csicsvari, J., Hirase, H., Czurko, A., Mamiya, A. & Buzsáki, G. Oscillatory coupling of hippocampal pyramidal cells and interneurons in the behaving rat. *J. Neurosci.* **19,** 274–287 (1999).
25. Jensen, O. & Lisman, J. E. Position reconstruction from an ensemble of hippocampal place cells: contribution of theta phase coding. *J. Neurophysiol.* **83,** 2602–2609 (2000).
26. deCharms, R. C. & Zador, A. Neural representation and the cortical code. *Annu. Rev. Neurosci.* **23,** 613–647 (2000).
27. Wood, E. R., Dudchenko, P. A. & Eichenbaum, H. The global record of memory in hippocampal neuronal activity. *Nature* **397,** 613–616 (1999).
28. Harris, K. D., Henze, D. A., Csicsvari, J., Hirase, H. & Buzsáki, G. Accuracy of tetrode spike separation as determined by simultaneous intracellular and extracellular measurements. *J. Neurophysiol.* **84,** 401–414 (2000).
29. Quirk, M. C. & Wilson, M. A. Interaction between spike waveform classification and temporal sequence detection. *J. Neurosci. Methods* **94,** 41–52 (1999).
30. Harris, K. D., Hirase, H., Leinekugel, X., Henze, D. A. & Buzsáki, G. Temporal interaction between single spikes and complex spike bursts in hippocampal pyramidal cells. *Neuron* **32,** 141–149 (2001).

Supplementary Information accompanies the paper on **www.nature.com/nature**.

Acknowledgements We thank J. E. Lisman, D. L. Buhl, S. M. Montgomery, P. E. Bartho and I. Creese for comments on the manuscript. This work was supported by grants from the National Institutes of Health

Competing interests statement The authors declare that they have no competing financial interests.

Correspondence and requests for materials should be addressed to G.B. (buzsaki@axon.rutgers.edu).

Role of the prolyl isomerase Pin1 in protecting against age-dependent neurodegeneration

Yih-Cherng Liou[1]*†, Anyang Sun[1,2]*, Akihide Ryo[1]†, Xiao Zhen Zhou[1], Zhao-Xue Yu[3], Han-Kuei Huang[4], Takafumi Uchida[5], Roderick Bronson[6], Guoying Bing[2], Xiaojiang Li[3], Tony Hunter[4] & Kun Ping Lu[1]

[1]*Cancer Biology Program, Department of Medicine, Beth Israel Deaconess Medical Center, Harvard Medical School, Boston, Massachusetts 02215, USA*
[2]*Department of Anatomy & Neurobiology, University of Kentucky, Lexington, Kentucky 40536, USA*
[3]*Department of Human Genetics, Emory University, Atlanta, Georgia 30322, USA*
[4]*Molecular and Cell Biology Laboratory, Salk Institute, La Jolla, California 92037, USA*
[5]*Department of Pathology, Tohoku University, Sendai 980-8575, Japan*
[6]*Tufts University School of Veterinary Medicine, Boston, Massachusetts 01536, USA*

* These authors contributed equally to this work
† Present address: Department of Biochemistry, National University of Singapore, 117597, Singapore (Y.-C.L.); Department of Pathology, Yokohama City University, Kanagawa 236-0004, Japan (A.R.)

The neuropathological hallmarks of Alzheimer's disease and other tauopathies include senile plaques and/or neurofibrillary tangles[1–4]. Although mouse models have been created by over-expressing specific proteins including β-amyloid precursor protein, presenilin and tau[1–10], no model has been generated by gene knockout. Phosphorylation of tau and other proteins on serine or threonine residues preceding proline seems to precede tangle formation and neurodegeneration in Alzheimer's disease[11–14]. Notably, these phospho(Ser/Thr)-Pro motifs exist in two distinct conformations, whose conversion in some proteins is catalysed by the Pin1 prolyl isomerase[15–17]. Pin1 activity can directly restore the conformation and function of phosphorylated tau or it can do so indirectly by promoting its dephosphorylation, which suggests that Pin1 is involved in neurodegeneration[14,18,19]; however, genetic evidence is lacking. Here we show that Pin1 expression is inversely correlated with predicted neuronal vulnerability and actual neurofibrillary degeneration in Alzheimer's disease. *Pin1* knockout in mice causes progressive age-dependent neuropathy characterized by motor and behavioural deficits, tau hyperphosphorylation, tau filament formation and neuronal degeneration. Thus, Pin1 is pivotal in protecting against age-dependent neurodegeneration, providing insight into the pathogenesis and treatment of Alzheimer's disease and other tauopathies.

Pin1-catalysed prolyl isomerization can regulate the function and/or dephosphorylation of some phosphoproteins, many of which are also recognized by the mitosis- and phosphorylation-specific monoclonal antibody MPM-2. Notably, induction of MPM-2 epitopes is a prominent common feature of Alzheimer's disease (AD), frontotemporal dementia with Parkinsonism linked to chromosome 17, Down's syndrome, corticobasal degeneration, progressive supranuclear palsy and Pick's disease[13,14]. In fact, the pattern of tau phosphorylation in AD is similar to that in mitotic cells[12,14]. Taking these observations together with the reduced amount of soluble Pin1 in brains at a late stage of AD[18], we previously proposed that Pin1 might protect against neurodegeneration[14,18]. However, it has been reported that in AD hippocampal expression of Pin1 occurs primarily in a few tangle-free degenerative neurons in CA1 and CA2, and not in CA3 and CA4 non-degenerative neurons, and it has been proposed that Pin1 promotes neurodegeneration[20]. Thus, the neuronal function of Pin1 remains elusive.

Neurons in different subregions of the hippocampus and neo-

cortex are known to have differential vulnerability to neurofibrillary degeneration in AD[21]. To examine the relationship between this predicted vulnerability and Pin1 expression, we examined the expression of Pin1 in normal human hippocampus and parietal cortex by immunostaining. Pin1 was detected in the cytoplasm and the nucleus of neurons (ref. 18 and Fig. 1). Notably, Pin1 expression showed an obvious subregional difference in all sections from eight normal brains (Fig. 1a and Supplementary Figs S1a and S2). In the hippocampus, expression of Pin1 was relatively higher in CA4, CA3, CA2 and presubiculum, and lower in CA1 and subiculum. In the parietal cortex, expression of Pin1 was relatively higher in layer IIIb-c neurons, and lower in layer V neurons (Supplementary Fig. S3a). The subregions with low expression of Pin1 are known to be prone to neurofibrillary degeneration in AD, whereas those containing high Pin1 expression are spared, suggesting that there is an inverse correlation between Pin1 expression and predicted vulnerability.

To extend this correlation, we immunostained ten AD-affected brain sections with both antibodies against Pin1 and a phospho-Tau antibody AT8 that detects early neurofibrillary degeneration. Tangle-bearing neurons were enriched in CA1 and subiculum of the hippocampus and in layer V of the parietal cortex (Fig. 1b and Supplementary Figs S1b and S3b). We also observed very high Pin1 immunoreactivity in cytoplasmic granules in a few neurons, mainly in CA1 (data not shown), which is probably due to the sequestration of Pin1 by strong MPM-2 epitopes in these granules[20].

In contrast to previous data[20], however, we found that Pin1 expression was readily detected in CA3 and CA4 subregions and, in fact, was higher in these regions than in tangle-rich subregions (Fig. 1b and Supplementary Fig. S1b). Overall, 96% of pyramidal neurons that contained relatively more Pin1 lacked tangles, whereas 71% of neurons that contained relatively less Pin1 had tangles (Fig. 1c). Even in the tangle-prone CA1 and subiculum of the hippocampus, expression of Pin1 was still lower in most tangle-bearing neurons than in tangle-free neurons (Fig. 1d). Expression of Pin1 was also relatively higher in tangle-sparing layer IIIb-c neurons, and lower in tangle-rich layer V neurons in parietal cortex (Supplementary Fig. S3b). These results suggest that there is an inverse correlation between Pin1 expression and actual neurofibrillary degeneration in AD.

The above results suggest that Pin1 might protect against neurodegeneration. To test this idea, we examined the neuronal phenotypes of *Pin1* $^{-/-}$ mice. These mice develop several age-dependent phenotypes, including retinal atrophy[22]. Because retinal atrophy can

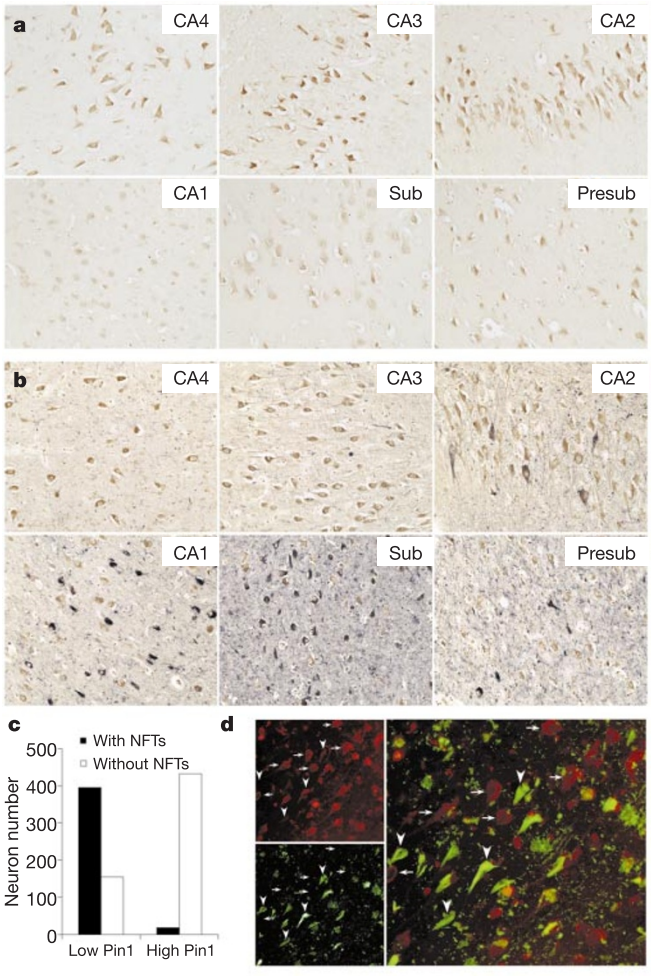

Figure 1 Inverse correlation of Pin1 expression with predicted neuronal vulnerability in normally aged brains and actual neurofibrillary degeneration in AD. **a**, **b**, Hippocampal sections from normal (**a**) or AD (**b**) brains were immunostained with antibodies against Pin1 (**a**) or antibodies against Pin1 (brown) and AT8 (purple) (**b**). **c**, Relationship between Pin1 immunoreactivity and NFTs in AD hippocampus. About 1,000 pyramidal neurons in AD were randomly selected and evaluated for AT8-positive or AT8-negative neurons, and Pin1-light (low) or Pin1-intense (high) immunoreactivity. **d**, Relationship between Pin1 immunoreactivity and NFTs in tangle-rich CA1 region detected by antibodies against Pin1 (red) and AT8 (green), respectively. Pin1 expression in most tangle-bearing neurons (arrowheads) was lower than that in tangle-free neurons (arrows).

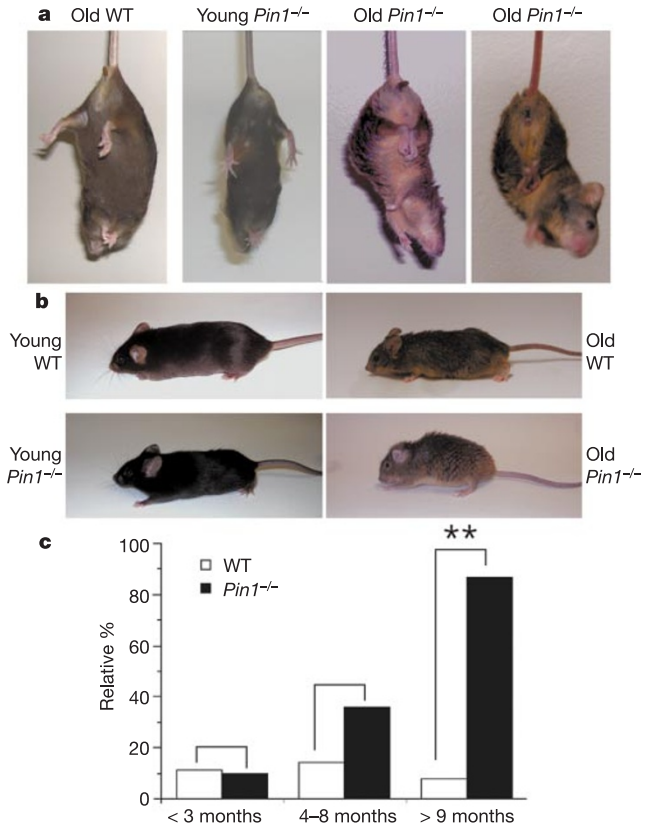

Figure 2 Age-dependent motor and behavioural deficits in *Pin1* $^{-/-}$ mice. **a**, Abnormal limb-clasping reflexes in old *Pin1* $^{-/-}$ mice. When lifted by the tail, young wild-type and *Pin1* $^{-/-}$ mice (2–3 months) and old wild-type mice (9–14 months) acted normally by extending their hind limbs and body, but old *Pin1* $^{-/-}$ mice flexed their legs to the trunk or tightened the back limbs to their bodies. **b**, Hunched postures shown by old *Pin1* $^{-/-}$ mice, but not by young *Pin1* $^{-/-}$ or any wild-type mice. **c**, Age-dependent motor disturbance. More than ten mice at different ages were placed on a hanging bar, and the percentage of the mice that fell off during the 1-min test period was recorded. Double asterisk, $P < 0.01$.

be a feature of neurodegeneration, we thought that *Pin1*$^{-/-}$ mice might show other neuronal phenotypes. Indeed, *Pin1*$^{-/-}$ mice, but not their wild-type littermates, showed progressive age-dependent motor and behavioural deficits, which included abnormal limb-clasping reflexes (Fig. 2a), hunched postures (Fig. 2b), reduced mobility and eye irritation. When subjected to a hang test[6], most old, but not young, *Pin1*$^{-/-}$ mice fell after grasping the rope only briefly (Fig. 2c). Thus, *Pin1*$^{-/-}$ mice develop progressive age-dependent motor and behavioural deficits, as do tau transgenic mice[6,10].

We examined whether *Pin1*$^{-/-}$ mice show age-dependent neuronal loss. The number of NeuN (neuron-specific nuclear protein)-positive neurons was significantly decreased in the parietal cortex of old, but not young, *Pin1*$^{-/-}$ mice (Fig. 3a, b). A similar neuronal degeneration was found in spinal cords of *Pin1*$^{-/-}$ mice (Supplementary Fig. S4a, b). Nissl staining also confirmed neuronal degeneration, as shown by the abnormally stained cytoarchitecture of *Pin1*$^{-/-}$ neurons (Supplementary Fig. S4c, arrows). Some *Pin1*$^{-/-}$ neurons had swollen cell bodies (data not shown), as observed in tau transgenic mice[10]; however, no obvious neuronal loss was found in other brain regions, notably cerebellum (data not shown), although there was *Pin1* expression in wild-type mice (Supplementary Fig. S5).

We used electron microscopy to confirm degeneration. In contrast to wild-type neurons (Fig. 3c), many *Pin1*$^{-/-}$ neurons showed dark, degenerating granules or organelles adjacent to the nucleus (Fig. 3d) and often had autophagic vacuoles (Fig. 3e), consistent with degenerated lysosomes. Degeneration was also observed in some axons (Fig. 3f). Another notable change found mostly in *Pin1*$^{-/-}$ neuronal processes, but not in wild-type controls, was the presence of electron-dense structures comprising compact and radiating filament-like structures without other visible organelles or vesicles (Fig. 3g, h). These ultrastructural changes confirm that there is degeneration in *Pin1*$^{-/-}$ neurons.

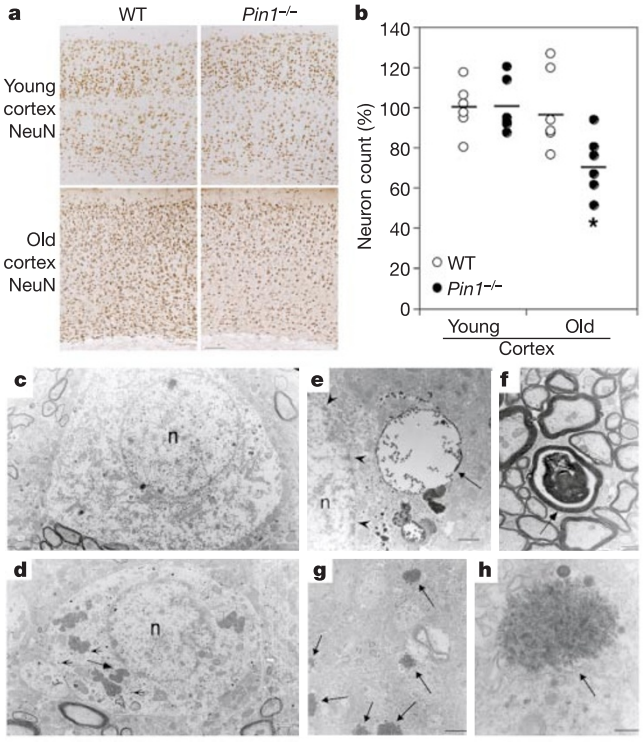

Figure 3 Age-dependent neuronal degeneration in *Pin1*$^{-/-}$ mice. **a**, **b**, Matched parietal cortex from wild-type and *Pin1*$^{-/-}$ mice was stained for NeuN (**a**) and neurons were counted (**b**). Asterisk, $P < 0.01$. **c**–**h**, Ultrastructure and AT8 immunogold labelling of degenerative neurons in *Pin1*$^{-/-}$ hippocampus. **c**, Wild-type neuron not labelled by AT8. **d**, *Pin1*$^{-/-}$ neuron labelled with AT8 immunogold (short arrows) and containing dark and degenerated organelles (long arrows) in the cytoplasm and near the nucleus (n). **e**, Autophagic vacuole (arrow) near the nuclear membrane (arrowheads). **f**, Axon degeneration (arrow). **g**, **h**, Neuron containing several compact and radiating structures (arrows, **g**) composed of radiating filament-like structures (arrow, **h**). Scale bars, 100 μm (**a**); 0.6 μm (**c**, **d**); 1.2 μm (**e**, **f**); 2 μm (**g**); 355 nm (**h**).

The findings that *Pin1*$^{-/-}$ mice develop neuronal degeneration in an age-dependent manner in some brain regions suggest that the effects are specific. The ability of Pin1 to promote dephosphorylation of MPM-2 epitopes[19] suggests that the deletion of *Pin1* might lead to an accumulation of MPM-2 epitopes, which is an early common characteristic of AD and related disorders[12,14,23]. Indeed, total MPM-2 reactivity was about threefold higher in *Pin1*$^{-/-}$ brain lysates than in control brain lysates (Fig. 4a), a result that was confirmed by immunostaining (Fig. 4g). These results indicate that *Pin1* knockout leads to neuronal induction of MPM-2 epitopes.

To examine the mechanisms underlying neurodegeneration, we focused on tau for the following reasons. First, tau-related pathologies are a hallmark of AD and other tauopathies[2,3] and have been characterized in mice[5–10]; notably, the phenotypes of transgenic tau mice are similar to those of *Pin1*$^{-/-}$ mice. Second, tau is a principal MPM-2 antigen[13] and a well-characterized substrate of Pin1 (refs 18, 19). Pin1 specifically acts on the phospho(Thr 231)-Pro motif in tau and induces a conformational change, thereby restoring tau function and promoting its dephosphorylation through the conformational specificity of phosphatases such as PP2A[18,19]. Reducing PP2A activity also increases phosphorylation in tau in mice[24]. Thus, tau might be aberrantly phosphorylated and show abnormal conformations in *Pin1*$^{-/-}$ mice. To examine this possibility, we isolated sarcosyl-insoluble extracts from brains of *Pin1*$^{-/-}$ and wild-type mice and analysed them by immunoblotting (Fig. 4b–f).

All sarcosyl-insoluble tau isoforms from *Pin1*$^{-/-}$ mice had much slower mobility on SDS gels than did wild-type controls (Fig. 4b), suggesting an increase in the total phosphorylation of tau. This was confirmed by phosphatase treatment and immunoblotting with phospho-specific monoclonal antibodies against tau (Fig. 4c, d). AT8 and AT180 strongly recognized the slower migrating tau isoforms, whereas TG3 selectively recognized the slowest migrating tau species (relative molecular mass ~68,000; $M_r \approx 68$K), which was also recognized by PHF-1 (Fig. 4d). The TG3 epitope was also induced in an age-dependent manner, and phosphatase treatment significantly, although not completely, reduced the TG3 signal (Fig. 4e, f). Finally, the 68K form of tau in *Pin1*$^{-/-}$ brains was also strongly recognized by Alz50 and MC1 (Fig. 4d), which detect neurofibrillary tangle (NFT)-specific conformations[25,26].

These results indicate that the 68K form of tau in *Pin1*$^{-/-}$ brain is hyperphosphorylated and contains NFT conformations. Of note, tau in NFTs of AD is notoriously resistant to complete dephosphorylation[27] and a similar 68K species (A68) in human AD is the defining component of paired helical filaments (PHFs) and is also recognized by Alz50 (refs 25, 26). Immunostaining showed strong immunoreactivity towards AT180, AT8, MC1 and Alz50 in the somatodendritic region of *Pin1*$^{-/-}$, but not wild-type, neurons in the parietal cortex, hippocampus, brainstem and spinal cord (Fig. 4g). The presence of phospho-Tau in the cytoplasm and axons of *Pin1*$^{-/-}$, but not wild-type, neurons was confirmed by immunogold electron microscopy (Fig. 3c, d and Supplementary Fig. S6). These results indicate that *Pin1* knockout causes age-dependent tau hyperphosphorylation and NFT-specific conformations.

To explore the mechanisms that induce MPM-2 and tau phosphoepitopes, we compared protein kinase and phosphatase activity in *Pin1*$^{-/-}$ and wild-type brains. Although there was no significant increase in the activity of total kinases, cyclin-dependent kinases (CDKs) or glycogen synthase kinase 3β (GSK-3β; Supplementary Fig. S7a, b), there was a significant decrease in phosphatase activity towards phospho(Ser/Thr)-Pro motifs in tau, but

not towards a non-phospho(Ser/Thr)-Pro phosphopeptide, in *Pin1*$^{-/-}$ brain lysates before obvious neurodegeneration (Fig. 4h). These results indicate that Pin1 specifically affects the dephosphorylation of phospho(Ser/Thr)-Pro motifs, consistent with the idea that Pin1 is required for efficient dephosphorylation of tau[19].

The findings that *Pin1*$^{-/-}$ neurons are strongly immunoreactive towards phospho- or NFT-specific monoclonal antibodies against tau suggests that they might contain tau filaments. To examine this possibility, we used Gallyas silver staining and thioflavin-S staining to detect NFTs[6,9,29]. In *Pin1*$^{-/-}$ mice (Fig. 5b–d), but not in wild-type controls (Fig. 5a), we observed some Gallyas-positive neurons in the hippocampus, thalamus and brainstem. In addition, a few *Pin1*$^{-/-}$, but not wild-type, neurons in the hippocampus, spinal cord and especially entorhinal cortex (ERC) were also positive for thioflavin-S staining (Fig. 5h); this positive staining was observed in four out of seven old *Pin1*$^{-/-}$ mice, but not in six wild-type mice examined. Notably, the pattern of thioflavin-S staining was similar to that observed in tau transgenic mice[10].

These results show that *Pin1*$^{-/-}$ neurons have NFT-like pathologies. Our attempt to visualize NFTs by *in situ* electron microscopy failed, possibly because the number of NFTs and/or neurons that developed late stages of NFTs was low, as indicated by thioflavin-S staining (Fig. 5e–h). To confirm the formation of tau filaments, we subjected sarcosyl-insoluble tau isolated from brain extracts to electron microscopy and immunogold electron microscopy. In extracts from 8 out of 12 old *Pin1*$^{-/-}$ brains, but not wild-type brains, we readily found filaments that were twisted or straight and about 15-nm wide (Fig. 5i, j). Further immunogold electron microscopy showed that the filaments were labelled with AT8 and AT180 (Fig. 5k, l), confirming that they were tau filaments. These results show that loss of Pin1 function causes the formation of endogenous tau filaments in mice.

In summary, we have shown that Pin1 expression inversely correlates with neuronal vulnerability in normal brain, and also with neurofibrillary degeneration in AD-affected brain. In addition, *Pin1*$^{-/-}$ mice develop age-dependent neuropathy, which is characterized clinically by motor and behavioural deficits and pathologically by tau hyperphosphorylation, tau filament formation and

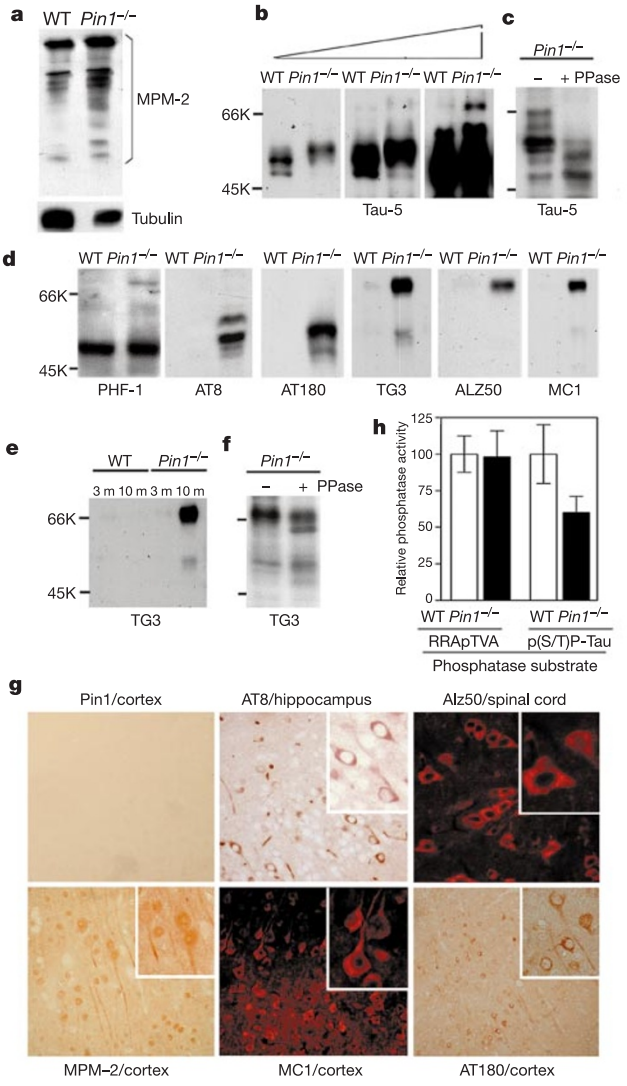

Figure 4 MPM-2 induction, tau hyperphosphorylation, NFT-specific conformations and reduced phosphatase activity toward the phospho(Ser/Thr)-Pro motif in *Pin1*$^{-/-}$ brain. **a**, Soluble brain extracts from age-matched old wild-type and *Pin1*$^{-/-}$ mice were analysed by immunoblotting with MPM-2. **b**, **d**, Sarcosyl-insoluble fractions were prepared from age-matched wild-type and *Pin1*$^{-/-}$ brains and analysed by immunoblotting with Tau-5 monoclonal antibodies against total tau (**b**) or various phosphorylation- and/or NFT-specific monoclonal antibodies against tau (**d**). **c**, **f**, Sarcosyl-insoluble tau was pretreated with phosphatases before being analysed by immunoblotting. **e**, Age-dependent induction of the TG3 epitope. **g**, Subcellular localization of MPM-2 epitopes, tau phosphoepitopes and NFT-conformation epitopes in *Pin1*$^{-/-}$ neurons, as determined by immunostaining. There was no positive staining in wild-type neurons (not shown). **h**, Activity towards phospho(Ser/Thr)-Pro motifs, but not towards a non-phospho(Ser/Thr)-Pro motif, is lower in brain lysates from 7-month-old *Pin1*$^{-/-}$ mice than in those from wild-type controls, as assayed with the indicated substrates.

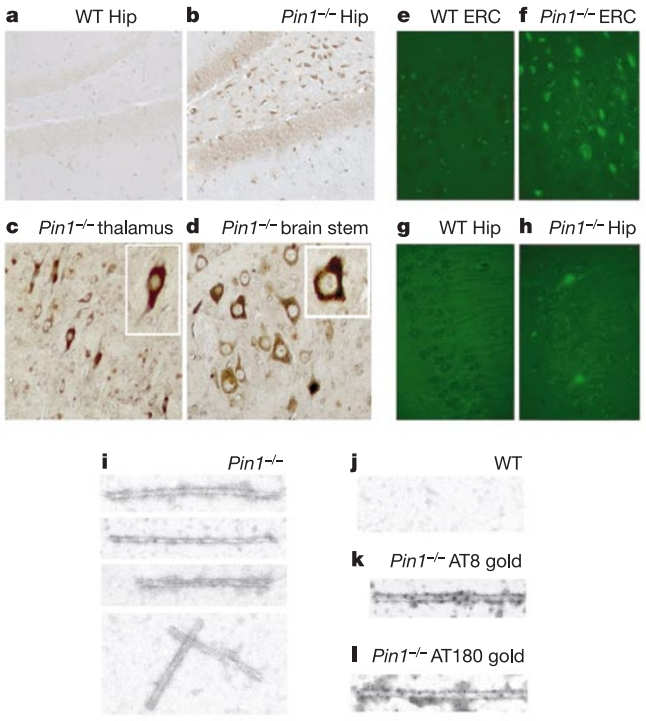

Figure 5 NFT-like pathologies and tau filaments in *Pin1*$^{-/-}$ neurons. **a**–**d**, Positive Gallyas silver staining of *Pin1*$^{-/-}$ neurons. Different regions of old wild-type (**a**) or *Pin1*$^{-/-}$ (**b**–**d**) brains were subjected to Gallyas silver staining. **e**–**h**, Positive thioflavin-S staining of *Pin1*$^{-/-}$ neurons. Different regions of old wild-type (**e**, **g**) or *Pin1*$^{-/-}$ (**f**, **h**) brains were subjected to thioflavin-S staining. **i**–**j**, Tau filaments isolated from *Pin1*$^{-/-}$ brains. Sarcosyl-insoluble extracts were prepared from old *Pin1*$^{-/-}$ (**i**) and wild-type (**j**) mice and examined by electron microscopy. **k**, **l**, Phosphorylated tau in the filaments. Sarcosyl-insoluble extracts were subjected to immunogold staining with AT8 (**k**) or AT180 (**l**) and then examined by electron microscopy. ERC, entorhinal cortex; Hip, hippocampus.

neuronal degeneration in brain and spinal cord. Notably, many of these neuronal phenotypes are highly similar to those induced by transgenic overexpression of tau or its mutants[5–10]. These results provide genetic evidence for the critical role of Pin1 in protecting against age-dependent neurodegeneration. To our knowledge, this is the first clear demonstration that endogenous mouse tau can form tau filaments. Thus, Pin1 is the first protein whose deletion has been shown to cause age-dependent neurodegeneration and tau pathologies. In addition, our finding that Pin1-mediated post-phosphorylation regulation is pivotal in maintaining normal neuronal function underscores the role of protein phosphorylation in neurodegenerative diseases and offers insight into the pathogenesis and treatment of AD and other tauopathies.

Given the phenotypic similarity between *Pin1*$^{-/-}$ and tau transgenic mice, tau-related pathologies are probably important in *Pin1*$^{-/-}$-induced neurodegeneration, although other Pin1-related deficits might also contribute to this process[22]. Manipulation of either tau kinases or phosphatases has been shown to increase phospho-Tau in mice[14,24,29,30]. We have now shown that deletion of *Pin1* reduces phosphatase activity specifically towards phospho(-Ser/Thr)-Pro motifs and induces tau hyperphosphorylation, NFT conformations and tau filament formation. These results suggest that tau is normally regulated by dynamic phosphorylation and dephosphorylation. If Pin1 function is low, as in the CA1 region of AD-affected brains, or absent, as in *Pin1*$^{-/-}$ mice, some phospho(-Ser/Thr)-Pro motifs in phospho-Tau might not be isomerized and thus exist in aberrant conformations. As a result, phospho-Tau would not be properly dephosphorylated and/or functionally restored, leading to tau hyperphosphorylation, NFT formation and neurodegeneration.

Although there is clear evidence of the age-dependent accumulation of abnormal and hyperphosphorylated tau, tau filaments and neurodegeneration in *Pin1*$^{-/-}$ brains, the patterns are not exactly identical to those observed in human AD or in human tau transgenic models. This might be due to differences in tau isoforms in mice or might reflect differences in the phosphorylation and aggregation of mouse tau. In addition, multiple and interactive factors probably contribute to tau hyperphosphorylation and neurodegeneration in human AD, and these factors might not be present in *Pin1*$^{-/-}$ mice. Further studies, including crossing *Pin1*$^{-/-}$ and *Pin1* transgenic mice with existing mouse models of amyloid-β or tauopathy, should help to elucidate the molecular mechanisms of AD and other tauopathies and might lead to the development of new therapies. □

Methods

Human samples and *Pin1*$^{-/-}$ mouse strains

Paraffin-embedded human samples of the hippocampus and parietal cortex were a gift from the Alzheimer's Disease Research Center (University of Kentucky) and consisted of ten cases of AD and eight controls, with a mean age at death of 78 ± 9 years and 79 ± 9 years, respectively. The mean postmortem intervals were 2.8 h for AD and 2.9 h for controls. All AD subjects met the clinical and neuropathological National Institute on Aging-Reagan Institute (NIA-RI) criteria for AD. Control subjects had no evidence of neurological disorders. Our study using human samples has been approved by our Institutional Review Board. The *Pin1*$^{-/-}$ mice are on a mixed 129/Sv and C57L/B6 background[22,28]. Young and old mice were 2–3 and 9–14 months, respectively. All results were reproduced in several mice.

Immunohistochemistry and immunofluorescent staining

We carried out conventional immunohistochemistry on human samples by using affinity-purified polyclonal and monoclonal antibodies against Pin1, as described[18]. For double-labelling experiments, sections were stained first with antibodies against Pin1 (brown), and then with AT8, which was visualized by the nickel-intensifying method (purple). For immunofluorescent double immunostaining, sections were incubated with an affinity-purified antibody against Pin1 and a monoclonal antibody against AT8, which were visualized by Cy3- and fluorescein isothiocyanate (FITC)-conjugated secondary antibodies. For mouse tissues, deparaffinized or floating brain sections were immunostained with various antibodies using an ABC kit (Vector Labs) or Cy3-conjugated secondary antibodies[22].

Immunoblot analysis

We prepared sarcosyl-insoluble extracts as described[7,8,10]. In brief, brain tissues were homogenized in a buffer containing 10 mM Tris-HCl (pH 7.4), 0.8 M NaCl, 1 mM EGTA and 10% sucrose. After centrifugation, the supernatants were added to 1% *N*-lauroylsarcosinate, and sarcosyl-insoluble extracts were collected by centrifugation and analysed by immunoblotting[18]. Alz50, MC1, TG3 and PHF-1 monoclonal antibodies against tau were a gift from P. Davies (Albert Einstein College of Medicine). AT8 and AT180 (Innogenetics) and Tau-5 (Biosource) antibodies were purchased. Tau-5 is specific for both phosphorylated and non-phosphorylated tau, PHF-1 for phosphoSer-396 and phosphoSer-404, AT8 for phosphoSer-199 and phosphoSer-202, AT180 for phosphoThr-231, TG3 for phosphoThr-231 in a NFT-specific conformation, and Alz50 and MC1 for NFT-specific conformations.

Hang test, neuron count and Nissl staining

We carried out the hang test, neuronal counting and Nissl staining as described[5,6]. For counting neurons, coronal sections at different regions of brains from age-matched *Pin1*$^{-/-}$ and wild-type littermates were processed in parallel for NeuN staining. The inner layer of the parietal cortex (S1BF) at 1.8-mm posterior to Bregma was selected, neurons were counted in comparable areas of each mouse, and an average number of two adjacent fields were obtained for each region of each mouse. For the spinal cord, the numbers of large neurons per anterior horn were counted and an average of two nearby sections was calculated for each mouse.

Kinase and phosphatase assays

We assayed total kinase activity in brain lysates by autophosphorylation in the presence of Mg^{2+} and [γ-^{32}P]ATP, and assayed CDK and GSK-3β activity towards tau after purification with $p13^{suc1}$ beads and antibodies against GSK-3β, respectively, as described[18]. Phosphatase activity towards the phosphopeptide RRApTVA (Promega; ref. 24) and phosphatase activity towards tau phosphorylated by Cdc2 (refs 18, 19) were assayed as described.

Gallyas silver staining and thioflavin-S staining

Gallyas silver staining[6] and thioflavin-S staining[10] were done as described.

Electron microscopy

To observe tau filaments, we resuspended sarcosyl-insoluble extracts isolated from *Pin1*$^{-/-}$ and control mouse brains and placed them on carbon-coated grids. The extracts were stained with phosphotungstic acid and observed by electron microscopy and immunogold electron microscopy with AT8 and AT180 (refs 7, 10).

Received 14 March; accepted 28 May 2003; doi:10.1038/nature01832.

1. Selkoe, D. J. The cell biology of β-amyloid precursor protein and presenilin in Alzheimer's disease. *Trends Cell Biol.* **8,** 447–453 (1998).
2. Mandelkow, E. M. & Mandelkow, E. Tau in Alzheimer's disease. *Trends Cell Biol.* **8,** 425–427 (1998).
3. Lee, V. M., Goedert, M. & Trojanowski, J. Q. Neurodegenerative tauopathies. *Annu. Rev. Neurosci.* **24,** 1121–1159 (2001).
4. Wong, P. C., Cai, H., Borchelt, D. R. & Price, D. L. Genetically engineered mouse models of neurodegenerative diseases. *Nature Neurosci.* **5,** 633–639 (2002).
5. Ishihara, T. *et al.* Age-dependent emergence and progression of a tauopathy in transgenic mice overexpressing the shortest human tau isoform. *Neuron* **24,** 751–762 (1999).
6. Lewis, J. *et al.* Neurofibrillary tangles, amyotrophy and progressive motor disturbance in mice expressing mutant (P301L) tau protein. *Nature Genet.* **25,** 402–405 (2000).
7. Gotz, J., Chen, F., Barmettler, R. & Nitsch, R. M. Tau filament formation in transgenic mice expressing P301L tau. *J. Biol. Chem.* **276,** 529–534 (2001).
8. Lewis, J. *et al.* Enhanced neurofibrillary degeneration in transgenic mice expressing mutant tau and APP. *Science* **293,** 1487–1491 (2001).
9. Gotz, J., Chen, F., van Dorpe, J. & Nitsch, R. M. Formation of neurofibrillary tangles in P301l tau transgenic mice induced by Aβ42 fibrils. *Science* **293,** 1491–1495 (2001).
10. Allen, B. *et al.* Abundant tau filaments and nonapoptotic neurodegeneration in transgenic mice expressing human P301S tau protein. *J. Neurosci.* **22,** 9340–9351 (2002).
11. Bancher, C. *et al.* Accumulation of abnormally phosphorylated tau precedes the formation of neurofibrillary tangles in Alzheimer's disease. *Brain Res.* **477,** 90–99 (1989).
12. Preuss, U. & Mandelkow, E. M. Mitotic phosphorylation of tau protein in neuronal cell lines resembles phosphorylation in Alzheimer's disease. *Eur. J. Cell Biol.* **76,** 176–184 (1998).
13. Vincent, I., Zheng, J. H., Dickson, D. W., Kress, Y. & Davies, P. Mitotic phosphoepitopes precede paired helical filaments in Alzheimer's disease. *Neurobiol. Aging* **19,** 287–296 (1998).
14. Lu, K. P., Liou, Y. C. & Vincent, I. Proline-directed phosphorylation and isomerization in mitotic regulation and in Alzheimer's disease. *BioEssays* **25,** 174–181 (2003).
15. Lu, K. P., Hanes, S. D. & Hunter, T. A human peptidyl-prolyl isomerase essential for regulation of mitosis. *Nature* **380,** 544–547 (1996).
16. Yaffe, M. B. *et al.* Sequence-specific and phosphorylation-dependent proline isomerization: a potential mitotic regulatory mechanism. *Science* **278,** 1957–1960 (1997).
17. Lu, K. P., Liou, Y. C. & Zhou, X. Z. Pinning down the proline-directed phosphorylation signaling. *Trends Cell Biol.* **12,** 164–172 (2002).
18. Lu, P. J., Wulf, G., Zhou, X. Z., Davies, P. & Lu, K. P. The prolyl isomerase Pin1 restores the function of Alzheimer-associated phosphorylated tau protein. *Nature* **399,** 784–788 (1999).
19. Zhou, X. Z. *et al.* Pin1-dependent prolyl isomerization regulates dephosphorylation of Cdc25C and tau proteins. *Mol. Cell* **6,** 873–883 (2000).
20. Holzer, M. *et al.* Inverse association of Pin1 and tau accumulation in Alzheimer's disease hippocampus. *Acta Neuropathol.* **104,** 471–481 (2002).
21. Davies, D. C., Horwood, N., Isaacs, S. L. & Mann, D. M. The effect of age and Alzheimer's disease on pyramidal neuron density in the individual fields of the hippocampal formation. *Acta Neuropathol.* **83,** 510–517 (1992).

22. Liou, Y. C. *et al.* Loss of Pin1 function in the mouse resembles the cyclin D1-null phenotypes. *Proc. Natl Acad. Sci. USA* **99,** 1335–1340 (2002).
23. Husseman, J. W., Nochlin, D. & Vincent, I. Mitotic activation: a convergent mechanism for a cohort of neurodegenerative diseases. *Neurobiol. Aging* **21,** 815–828 (2000).
24. Kins, S. *et al.* Reduced protein phosphatase 2A activity induces hyperphosphorylation and altered compartmentalization of tau in transgenic mice. *J. Biol. Chem.* **276,** 38193–38200 (2001).
25. Wolozin, B. L., Pruchnicki, A., Dickson, D. W. & Davies, P. A neuronal antigen in the brains of Alzheimer patients. *Science* **232,** 648–650 (1986).
26. Lee, V. M., Balin, B. J., Otvos, L. Jr & Trojanowski, J. Q. A68: a major subunit of paired helical filaments and derivatized forms of normal Tau. *Science* **251,** 675–678 (1991).
27. Gordon-Krajcer, W., Yang, L. & Ksiezak-Reding, H. Conformation of paired helical filaments blocks dephosphorylation of epitopes shared with fetal tau except Ser199/202 and Ser202/Thr205. *Brain Res.* **856,** 163–175 (2000).
28. Fujimori, F., Takahashi, K., Uchida, C. & Uchida, T. Mice lacking Pin1 develop normally, but are defective in entering cell cycle from G90) arrest. *Biochem. Biophys. Res. Commun* **265,** 658–663 (1999).
29. Patrick, G. N. *et al.* Conversion of p35 to p25 deregulates Cdk5 activity and promotes neurodegeneration. *Nature* **402,** 615–622 (1999).
30. Lucas, J. J. *et al.* Decreased nuclear β-catenin, tau hyperphosphorylation and neurodegeneration in GSK-3β conditional transgenic mice. *EMBO J.* **20,** 27–39 (2001).

Supplementary Information accompanies the paper on **www.nature.com/nature**.

Acknowledgements We thank F. Gage, L. Cantley, B. Neel and K. Kosik for comments on the manuscript; W. Markesbery for human brain samples; P. Davies for tau antibodies; and G. Liu, M. Liu and M. Ericsson for technical assistance. Y.-C.L. is a Fellow of the Canadian Institutes of Health Research, A.R. is a Special Fellow of the Leukemia and Lymphoma Society; T.H. is a Frank and Else Schilling American Cancer Society Research Professor; and K.P.L. is a Pew Scholar and a Leukemia and Lymphoma Society Scholar. This study was supported by NIH grants to G.B., X.J.L., T.H. and K.P.L.

Competing interests statement The authors declare competing financial interests: details accompany the paper on **www.nature.com/nature**.

Correspondence and requests for materials should be addressed to K.P.L. (klu@bidmc.harvard.edu).

Essential role for the peroxiredoxin Prdx1 in erythrocyte antioxidant defence and tumour suppression

Carola A. Neumann[1], Daniela S. Krause[1], Christopher V. Carman[1], Shampa Das[1], Devendra P. Dubey[1], Jennifer L. Abraham[1], Roderick T. Bronson[3], Yuko Fujiwara[2], Stuart H. Orkin[2] & Richard A. Van Etten[1]*

[1]*Center for Blood Research and Department of Genetics, Harvard Medical School, and*
[2]*Howard Hughes Medical Institute, Children's Hospital, Boston, Massachusetts 02115, USA*
[3]*Tufts University School of Veterinary Medicine, North Grafton, Massachusetts 01536, USA*

* Present address: Molecular Oncology Research Institute, Tufts-New England Medical Center, Boston, Massachusetts 02111, USA

Reactive oxygen species are involved in many cellular metabolic and signalling processes[1] and are thought to have a role in disease, particularly in carcinogenesis and ageing[2]. We have generated mice with targeted inactivation of *Prdx1*, a member of the peroxiredoxin family of antioxidant enzymes[3]. Here we show that mice lacking Prdx1 are viable and fertile but have a shortened lifespan owing to the development beginning at about 9 months of severe haemolytic anaemia and several malignant cancers, both of which are also observed at increased frequency in heterozygotes. The haemolytic anaemia is characterized by an increase in erythrocyte reactive oxygen species, leading to protein oxidation, haemoglobin instability, Heinz body formation and decreased erythrocyte lifespan. The malignancies include lymphomas, sarcomas and carcinomas, and are frequently associated with loss of Prdx1 expression in heterozygotes, which suggests that this protein functions as a tumour suppressor. Prdx1-deficient fibroblasts show decreased proliferation and increased sensitivity to oxidative DNA damage, whereas *Prdx1*-null mice have abnormalities in numbers, phenotype and function of natural killer cells. Our results implicate Prdx1 as an important defence against oxidants in ageing mice.

Cellular defences against reactive oxygen species (ROS) include enzymes such as superoxide dismutase (which converts superoxide to hydrogen peroxide), catalase and glutathione peroxidase (which convert hydrogen peroxide to water), as well as non-enzymatic scavengers such as glutathione, ascorbic acid and carotenoids. Peroxiredoxins (Prdxs), a family of small antioxidant proteins that contain essential catalytic cysteine residues and use thioredoxin as an electron donor[3], also scavenge peroxide and are thought to be involved in the cellular response to ROS. Prdxs are abundant proteins found in organisms from all three kingdoms, with at least five distinct members in mammals. Mammalian Prdx1, also known as Pag[4] or MSP23 (ref. 5), is a ubiquitously expressed protein with a relative molecular mass of 23,000 (23K) that is encoded by a single gene on human chromosome 1p34 (ref. 6) and mouse chromosome 4 (ref. 7) and induced by serum stimulation[4] and oxidative stress[5,8]. Transfection studies show that Prdx1 can eliminate peroxide *in vivo* and can regulate ROS induced by growth factor signalling[9]. In addition to its role as an antioxidant enzyme, Prdx1 has been independently isolated as an erythrocyte cytosolic protein that enhances the cytoxicity of natural killer (NK) cells[10], a

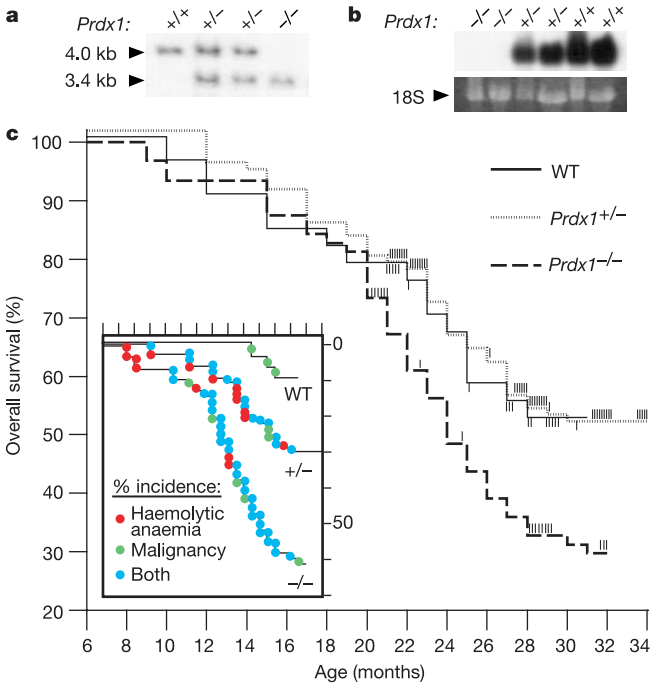

Figure 1 Premature death in ageing *Prdx1* $^{-/-}$ mice. **a**, Genotype of four littermates from a *Prdx1* $^{+/-}$ cross. Southern blot of *Spe*I-digested genomic DNA with a *Prdx1* exon II probe shows wild-type and mutant alleles of 4.0 and 3.4 kilobases, respectively. **b**, Northern blot of total liver RNA from six littermates hybridized with a *Prdx1* complementary DNA probe (top). Ethidium bromide staining of 18S rRNA (bottom) verifies equivalent loading. **c**, Kaplan–Meier survival curve of cohorts of wild-type ($n = 34$), *Prdx1* $^{+/-}$ ($n = 88$) and *Prdx1* $^{-/-}$ ($n = 64$) littermates on a mixed B6 × 129SvEv background. Mutant lines generated from three independently targeted ES cell clones were studied with similar results. The ages of surviving mice are indicated by tick marks. The difference in survival between wild-type and *Prdx1* $^{-/-}$ mice is statistically significant ($P = 0.05$, Mantel–Cox test). Inset, percentage of mice in these cohorts that developed haemolytic anaemia (red), malignancy (green) or both (blue). The *x* axis is identical to the main graph.